Applied Catalysis B: Environmental 138–139 (2013) 391–400

Contents lists available at SciVerse ScienceDirect

Applied Catalysis B: Environmental

journal homepage: www.elsevier.com/locate/apcatb

# Optimization of the degradation of imazalil by photocatalysis: Comparison between commercial and lab-made photocatalysts

Dunia E. Santiago[a,*], José M. Doña-Rodríguez[a,*], J. Araña[a], C. Fernández-Rodríguez[a], O. González-Díaz[a], J. Pérez-Peña[a], Adrián M.T. Silva[b]

[a] Grupo de Fotocatálisis y Espectroscopía Aplicada al Medioambiente-FEAM (Unidad Asociada al ICMSE, C.S.I.C.), CIDIA-Dpto. de Química, Edificio del Parque Científico Tecnológico, Universidad De Las Palmas De Gran Canaria, Campus Universitario de Tafira, 35017, Las Palmas, Spain
[b] LCM – Laboratory of Catalysis and Materials – Associate Laboratory LSRE/LCM, Faculdade de Engenharia, Universidade do Porto, Rua Dr. Roberto Frias, 4200-465, Porto, Portugal

ARTICLE INFO

*Article history:*
Received 26 December 2012
Received in revised form 1 March 2013
Accepted 5 March 2013
Available online 20 March 2013

*Keywords:*
Imazalil
Heterogeneous photocatalysis
Lab-made photocatalysts
$TiO_2$

ABSTRACT

The elimination and mineralization of the fungicide imazalil and its by-products has been studied by means of heterogeneous photocatalysis. The activity of different photocatalysts, including the commercial $TiO_2$ benchmark photocatalyst (Evonik P25) and several $TiO_2$-based lab-made catalysts, is compared. The best results were achieved with the new lab-made photocatalyst synthesized by using sulphuric acid in the sol–gel process and calcined at a high temperature (EST-1023t). The apparent initial rate constant was up to 2 times faster for EST-1023t when compared to that obtained with Evonik P25. The effect of different operating parameters (pH, photocatalyst load and initial imazalil concentration) on the photocatalytic process were studied for these two photocatalysts and a degradation pathway was proposed considering data obtained from ion chromatography, LC–MS and FTIR studies. The formation of imidazole acetic acids was confirmed, as well as complete mineralization and release of stoichiometric nitrogen (as ammonium and nitrate) and chloride ions.



## 1. Introduction

Conventional agriculture relies on the use of many types of pesticides (insecticides, fungicides, etc.) to satisfy the food demands from an increasing population. Imazalil is a fungicide that is being widely used in the postharvest of many fruits, including oranges, watermelons, lemons, bananas, among others [1]. Water contaminated with postharvest fungicides is normally washed away into the sewage system, generating environmental and health awareness due to the bioaccumulation and the toxic effects that these compounds produce in organisms. For this reason, many countries have established a legislation to control the pesticides that can be used and the tolerable amount in which they can be employed [2]. Such legislations are periodically revised and updated. In the particular case of Canary Islands (Spain), one of the biggest banana producing regions, legislation requires that the concentrations of pesticides must not exceed 0.05 mg/L both in wastewater and for irrigation purposes [3,4].

We have collected samples of postharvest wastewater from different banana cooperatives, finding imazalil concentrations between 1.32 and 38.19 mg/L. This wide range of concentrations is dependent on the way the company works, including the production rate, the amount of water they use to wash the fruit, and the frequency with which they renew this water. Generally, each cooperative implements a different postharvest treatment, depending on their mean annual productivity [5].

Conventional wastewater treatment plants, based on biological treatments, are unable to eliminate pesticides, due to the low biodegradability of these pollutants [6], in particular when they are present in high concentrations. For this reason, other processes must be established to treat these pesticides [7].

Advanced oxidation techniques represent an efficient alternative for the degradation of these pesticides, especially heterogeneous $TiO_2$-based photocatalysis [6,8,9], which is based on the production of •OH radicals [10].

Although many researchers have correlated the photocatalytic efficiency of $TiO_2$ with its particle size or anatase–rutile ratio, there are many other parameters that affect the photocatalytic process when using $TiO_2$, such as its surface area, crystallinity, band-gap and crystalline orientation [11].

Metal doping has been found to enhance the photocatalytic activity of different semiconductors, mainly due to the formation of a Schottky barrier at the interface of metals and $TiO_2$ that improves the separation of holes and electrons. Moreover, the holes act as a sink for electrons, preventing the accumulation of excess electrons

* Corresponding authors. Tel.: +34 928457301.
*E-mail addresses:* dsantiago@proyinves.ulpgc.es (D.E. Santiago), jdona@dqui.ulpgc.es (J.M. Doña-Rodríguez).

0926-3373/$ – see front matter © 2013 Elsevier B.V. All rights reserved.
http://dx.doi.org/10.1016/j.apcatb.2013.03.024

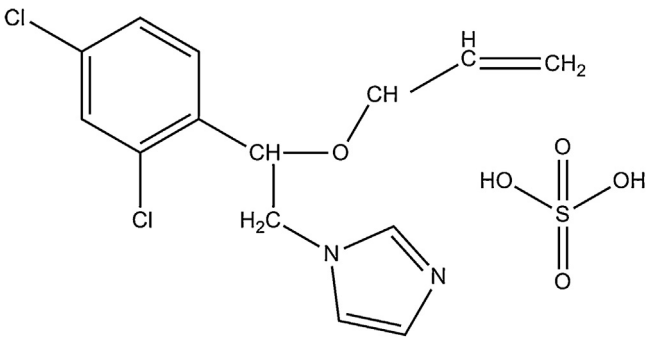

**Scheme 1.** Imazalil (sulphate).

on the surface of $TiO_2$, and the defect sites ($Ti^{3+}$), which are responsible for an efficient photocatalytic process. However, the doping of photocatalysts does not always lead to a positive effect. For instance, deposited Pt particles can reduce the adsorption of contaminants onto the photocatalyst, scatter the UV light to decrease the irradiation efficiency of $TiO_2$ and may also act as the recombination center for photoinduced holes and electrons [12,13].

The aim of this paper is to study the removal of imazalil from water by means of heterogeneous photocatalysis. For this purpose, several $TiO_2$-based catalysts, commercial and lab-made, tested for degradation of this pollutant. In addition, different operating conditions (pH, catalyst load, and initial imazalil concentration) were studied, the toxicity of reaction samples was assessed and reaction by-products were identified for the most active photocatalysts.

## 2. Materials and methods

### 2.1. Materials and chemicals

The photocatalysts used in the experiments and their properties are listed in Table 1.

Imazalil was used in a water-soluble form, as imazalil, a commercially available formulation (Fruitgard-IS-7.5). The imazalil molecule is presented in Scheme 1.

When needed, the solution pH was adjusted with diluted $H_2SO_4$ or NaOH solutions.

The commercial catalyst (Evonik P25) was provided by Evonik Industries AG (Germany).

ECT photocatalysts were synthesized by a sol–gel method [14]. For this, a solution containing 40 mL ethanol (99.5% Panreac) and 17 mL titanium butoxide (97% Sigma–Aldrich) was added drop by drop to 15 mL of a 0.3 M citric acid solution (99.5% Panreac) and 40 mL of ethanol (99.5% Panreac). The mixing time was 3 h. After this, the solution was stirred for 30 min and allowed to age for 48 h. The catalysts were then dried at 373 K for 24 h. After this aging and drying treatment, the catalysts were sieved with a 63 μm mesh. The smaller aggregates were then placed on porcelain capsules and calcined at 302 K/h until a final temperature of 773, 873 or 1023 K for catalysts ECT-773t, ECT-873t and ECT-1023t, respectively.

EST 1023t photocatalyst was also synthesized by a sol–gel procedure. In this case a solution containing 40 mL ethanol (99.5% Panreac) and 17 mL titanium butoxide (97% Sigma–Aldrich) was added drop by drop to 15 mL of a 0.6 M sulphuric acidic solution (96% Panreac) and 40 mL of ethanol. The acid used was sulphuric acid (99.5% Panreac). The mixing time was 2 h. After this, the final solution was stirred for 30 min and then allowed to age for 48 h. Then, the catalysts were dried at 373 K for 24 h. Subsequent to this aging and drying treatment, sieving was carried out using a 63 μm mesh size. For annealing treatment, catalysts were placed on porcelain capsules. A temperature programme with slope of 302 K/h was used and the final temperature (1023 K) was held for 3.5 h.

The difference between the photocatalysts EST-1023t and ECT-1023t is that the former one is synthesized using sulphuric acid and the latter one using citric acid. Submitting $TiO_2$ to high thermal treatments usually provokes the transformation of anatase to rutile, which is the thermodynamically stable phase at high temperatures, generally above 873 K [15]; however, for the photocatalyst EST-1023t and mostly for ECT-1023t the anatase to rutile transition is delayed. Some studies reveal that particle size is a key parameter controlling this transformation (ref 750). When comparing photocatalysts EST-1023t and ECT-1023t with Evonik P25 (Table 1) we observe a decrease in surface area with increasing particle size; this is most clearly seen for EST-1023t.The platinized samples were prepared by metal photodeposition following a method previously reported [16]. Pt deposition was achieved using hexachloroplatinic (IV) acid ($H_2PtCl_6$, Sigma–Aldrich 37.5% Pt). Solutions of $H_2PtCl_6$ (corresponding to a 1.0 wt.% metal loading) were prepared and mixed with suspensions of the $TiO_2$ in distilled water, adding a 0.3 M solution of isopropanol (98.5% Panreac), used as sacrificial donor. Photodeposition was performed at room temperature by illuminating the suspensions for 6 h with a medium pressure mercury lamp (400 W) ($8.1 \times 10^{-7}$ einstein/s L) while maintaining continuous stirring and nitrogen purging. The precipitate was filtered, washed with MilliQ water and then dried at 393 K for 2 h.

### 2.2. Analytical determinations

Concentrations of imazalil at different reaction times were HPLC-measured using a UV detector ($\lambda = 225$ nm), a Supelco Discovery C18 column (25 cm × 4.6 mm ID, 5 μm particles) and an acetonitrile-10 mM $KH_2PO_4$ solution (45:55) with 100 mg/L of sodium 1-octanesulfonate as mobile phase (adjusted to pH 3.0 with phosphoric acid). This method is a modification of that reported by different authors [17,18]. The quantification was performed by least-squares fit. The detection and quantification limits for imazalil were 0.05 mg/L and 0.15 mg/L, respectively. The adjusted $R^2$ was 0.998.

Analysis of intermediates was performed with a Varian System consisting of a 212-LC Binary Gradient LC/MS Chromatography Pump fitted with a Prostar 410 HPLC Autosampler and a 320-MS

**Table 1**
Characteristics of the different photocatalysts used in this work.

| Catalyst | Specific surface area ($m^2\ g^{-1}$) | Anatase/rutile ratio (%) | Crystalline size (nm) | | Band Gap (eV) |
|---|---|---|---|---|---|
| | | | Anatase | Rutile | |
| Evonik P25 | 52 | 80/20 | 22.0 | 25.0 | 3.18 |
| ECT-773t [14] | 38.4 | 100/0 | 21.7 | – | 3.19 |
| ECT-873t [14] | 27.8 | 100/0 | 36.9 | – | 3.19 |
| ECT-1023t [14] | 18.3 | 89–94/11–6 | 57.0 | 86.3 | 2.97 |
| EST-1023t | 13.51 | 70–80/30–20 | 62.3 | 96.1 | 2.96 |
| Evonik P25 + 1% Pt | 52 | 80/20 | 22.0 | 25.0 | – |
| ECT-1023t + 1% Pt | 15.8 | 89–94/6–11 | 57.0 | 86.3 | – |

LC/MS/MS system (triple quadrupole) equipped with an electrospray ionisation (ESI) interface. First a full scan was performed both in positive and negative mode, in order to identify the possible photoproducts. MS analysis was carried out in positive mode using an ion spray voltage of 1.5 kV. Ionization in the ESI source was achieved using nitrogen as a nebulizer (60° C, 65 psi) and drying gas (300 °C, 30 psi). Collision-induced dissociation (CID) was conducted with argon as the collision gas at a fixed pressure of 2 psi. The mobile phase consisted of water containing 0.2% formic acid and 5 mM ammonium formate (pH 2.6) (eluent A) and methanol (eluent B). For the determinations, a linear gradient was employed, from 95% A to 70% A and a column re-equilibration time of 5 min. The flow rate was 200 μL/min. The column used was a Varian Pursuit UPS 2.4 C18 (5 cm × 2.0 mm ID, particle size 2.4 μm).

Total organic carbon (TOC) was measured by using a TOC Shimadzu V-CSN.

The toxicity of samples was determined by using the MultiTox® *Vibrio fischeri* toxicity test. This bioassay was performed following standard UNE-EN-ISO 11348-3: 1998, which describes the determination of the inhibitory effect of water samples on the light emission of *V. fischeri* (luminescent bacteria test). Toxicity levels are determined by monitoring the decrease of luminescence due to inhibition of bacterial luciferase upon contact with toxic substances [19]. The equipment used for these measurements was an Optocomp I luminometer from MGM Instruments.

Toxicity was also evaluated by using the duckweed (*Lemna minor*) toxicity test [20]. Glass Petri dishes containing 12 ± 3 fronds of common duckweed (*L. minor*) were placed under constant visible radiation (one 18-W fluorescence tube placed approximately 25-cm above the test chambers) for 96 ± 2 h in a chamber with an ambient temperature of 25 ± 2 °C. Four replicates were used for each sample, i.e., a control without pollutant and samples with different pollutant concentrations. To 50 mL of solution, 0.5 mL of concentrated nutrient solutions were added. To each dish 15 mL of sample at pH 7.5–8 were added. Growth inhibition percentage (I) was calculated with respect to the control without pollutant according to: $I(\%) = 100(C - T)/C$, where $C$ and $T$ are the frond number mean increments for the control and the sample, respectively.

Ion chromatography was used to determine the concentration of chloride, ammonium and nitrate ions in solution. For this purpose, a DIONEX Ionic Chromatograph equipped with a GP50 gradient pump, ED50 electrochemical detector and an IonPac AS11-HC column (4 mm × 250 mm) was employed, using aqueous NaOH (30 mM) as eluent and a flow rate of 1 mL $min^{-1}$.

For the FTIR (Fourier Transform Infrared) determinations, the catalysts remained in contact with a 200 mg/L imazalil solution at different pH values during 24 h. FTIR studies were also performed at different reaction times, in order to verify the degradation mechanism proposed for the fungicide. After this, the catalyst was filtered and the remaining water was evaporated at room temperature. A FTIR Thermo Scientific Nicolet iS10 spectrometer was used for FTIR spectra. Intervals of 4000–1000 $cm^{-1}$ were used. These analyses were performed by placing films of the catalysts between two $CaF_2$ windows.

In addition, the point zero of charge ($pH_{PZC}$) of the photocatalyst EST-1023t was determined by adjusting the pH of 50 mL of a NaCl 0.01 M solution to a value between 2 and 12 by adding HCl 0.1 M or NaOH 0.1 M. Then 0.15 g of $TiO_2$ was added to each flask and the final pH was measured after 24 h of continuous stirring at room temperature [21].

For real particle size distribution measurements, a Beckman Coulter LS 13320 particle size analyzer equipped with a Universal Liquid Module was used along with the Fraunhofer optical model. The BET specific surface areas ($S_{BET}$) were determined from $N_2$ adsorption isotherms obtained at 77 K in a Micromeritics Gemini instrument. Band-gap values were determined from diffuse reflectance spectra.

### 2.3. Experimental conditions

Degradation tests were performed in 250 mL Pyrex glass batch reactors, filled with 200 mL of the pollutant aqueous solution and 1 g/L of photocatalyst. Aeration was maintained with an aquarium pump (EOLO AC3000 model: 2.5 W power, 2 L/min output and pressure >0.02 MPa) and a constant stirring of 450 rpm. A 60 W Philips Solarium HB175 equipped with four 15 W Philips CLEO fluorescent tubes with emission spectrum from 300 to 400 nm (maximum around 365 nm) and with an average irradiation power of about 9 mW was used as UV source in the photodegradation and mineralization studies. The lamp was turned on after established the adsorption equilibrium. Samples were taken to monitor the reaction in time intervals of 15 min during the first hour, and during 30 min thereafter. The samples were filtered using 0.45 μm syringe filters before analysis.

The tests were conducted at three different pH – 3.8 ± 0.1 (natural), 5.0 and 7.0 – in order to determine the most favorable pH for the degradation and mineralization of the fungicide. The best photocatalyst load was elected at the optimal pH.

The photocatalytic process was also studied for different imazalil initial concentrations in order to establish a relationship between concentration and other parameters influencing the degradation reaction.

A statistical treatment was performed for all the data presented in this work. The standard errors shown in every figure have been calculated by using 95% confidence limits.

## 3. Results and discussion

### 3.1. Photolysis of imazalil

Preliminary experiments were carried out to evaluate the possible photolysis effect on the photocatalytic process. We have observed that no significant effect is produced at acid pH, but imazalil was reduced by 19% and 32% at pH 7.0 in 60 and 120 min, respectively. The photolysis of imazalil at pH 7.0 has been already reported in datasheets from IUPAC Agrochemicals, FAO or EU Health&Consumer Protection Directorate [22,23].

### 3.2. Screening of photocatalysts

Photocatalytic degradation of imazalil seems to follow a pseudo-first-order kinetic and, thus, the apparent reaction rate constants were determined from the slope of the plot $\ln[C/C_0]$ vs. reaction time. Fig. 1 shows these apparent reaction rate constants determined for the degradation of imazalil ($k_{IMS}$), as well as the percentage of mineralization after 120 min of irradiation, when using 50 mg/L of imazalil, a solution pH of 5.0 and a load of 1 g/L for all the catalysts listed in Table 1.

It can be observed in Fig. 1 that $k_{IMS}$ and imazalil mineralization increase by increasing the calcination temperature of the lab-made catalysts, related to a consequent appearance of the rutile phase [24]. Taking into account the data provided in Table 1, we can also see that degradation rates increase with particle size. It has been reported that the most efficient $TiO_2$ photocatalysts in the degradation of non-adsorbed substrates are those with large particle size, high crystallinity and high anatase phase content [14].

We can also observe that there is a correlation with the band-gap values, as there is an increase in degradation and mineralization with decreasing band-gap. This enables the use of photons from higher wavelengths, or less energetic photons.

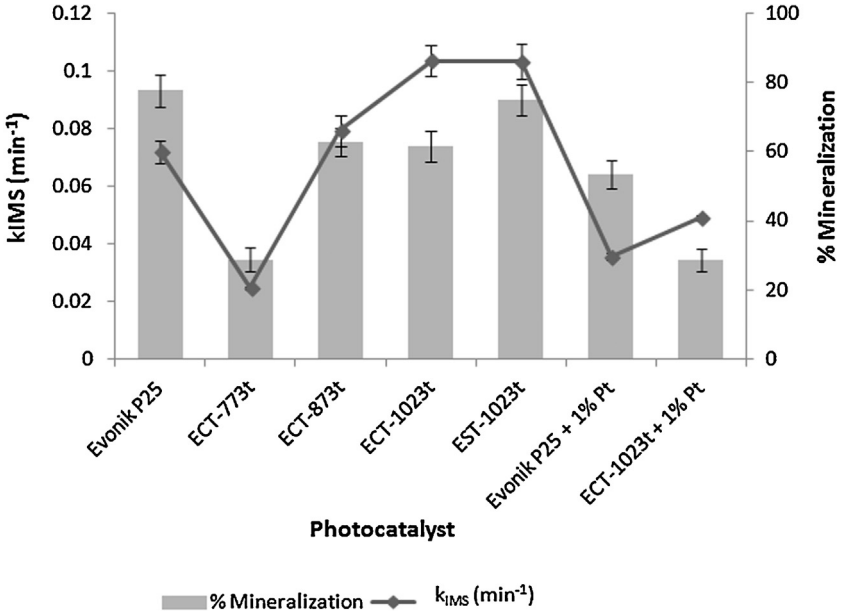


**Fig. 1.** Degradation rate constant and mineralization (%) of imazalil after 120 min irradiation using different photocatalysts.

It is noteworthy that $k_{IMS}$ is 1.43 and 1.44 times faster for EST-1023t and ECT-1023t, respectively, in comparison to the $k_{IMS}$ determined for the commercial Evonik P25 photocatalyst.

Furthermore, the addition of Pt to the photocatalysts resulted in a clear loss of efficiency, in accordance with previously reported works with phenol-type mechanisms [25].

Regarding mineralization in 120 min of irradiation, comparable results were obtained for Evonik P25 (80.4 ± 4.6%) and EST-1023t (76.3 ± 4.5%), but not for ECT-1023t, that only achieves 63.8 ± 4.3% of mineralization. The different behaviour observed for the photocatalyst ECT-1023t may be related to the very low content of rutile phase (Table 1), in comparison to Evonik P25 and EST-1023t, as many studies remark that the presence of rutile can enhance the photocatalytic activity of anatase in the degradation of organic contaminants [26].

### 3.3. Effect of pH

pH plays an important role in heterogeneous photocatalysis, since it determines the surface charge of the photocatalyst and the size of aggregates that are formed [27]. The photocatalytic degradation and mineralization (Fig. 2), of imazalil were studied at different reaction pH values for the three most efficient photocatalysts described above; that is: Evonik P25, ECT-1023t and EST-1023t. The pH values considered were natural pH (3.8 ± 0.1 ± 0.1), 5 and 7.

Degradation rates slightly increased when using commercial Evonik P25 at higher pH values (Fig. 2 – left), but this does not occur for the lab-made catalysts, where pH does not particularly seem to influence the degradation rate of imazalil.

**Table 2**
Particle size and $pH_{pzc}$ of the principal photocatalysts used in this work.

| Catalyst | $pH_{pzc}$ | Particle size (μm) |
|---|---|---|
| Evonik P25 | 6.5 | 3.9 |
| ECT-1023t [14] | 5.2 | 39.0 |
| EST-1023t | 6.2 | 30.1 |

Adsorption of imazalil on these three catalysts was also studied at different pH values (not shown), being observed that the adsorption for all the photocatalysts is disfavoured at lower pH values. This can be explained by the fact that the $pH_{PZC}$ of the studied photocatalysts are in the range of 5.0–6.5 (shown in Table 2), and imazalil is a weak base ($pK_a$ 6.54), like other imidazole compounds and imidazolium salts [23,28–30]. Therefore, at pH values below the $pH_{pzc}$ of the photocatalysts, these are positively charged, and imazalil is predominantly in its cationic form. In such conditions, electrostatic repulsion prevents adsorption of the pollutant. In contrast, at pH 7.0 (pH > $pK_a$), imazalil is mainly present in its neutral form and, therefore, its adsorption on the photocatalysts is higher.

Concerning the degradation of imazalil with the photocatalysts EST-1023t and ECT-1023t, we can observe in Fig. 2 that pH does not particularly influence this process. However, adsorption of imazalil on the photocatalysts is higher at pH 7 (between 9 ± 0.8 and 9.9 ± 0.1 mg/g) than at pH 3.8 ± 0.1 or 5 (between 1.5 ± 0.9 and 3.0 ± 0.9 mg/g). This suggests that adsorption does not significantly

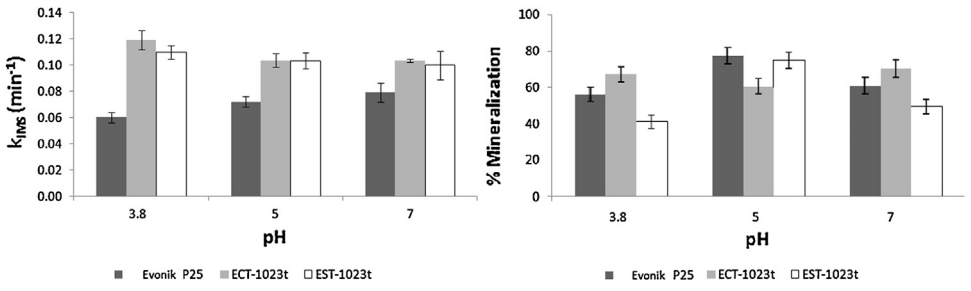


**Fig. 2.** Degradation rate constant (left) and % mineralization (right) for imazalil using three different photocatalysts (one commercial and two home-made) at different pH.

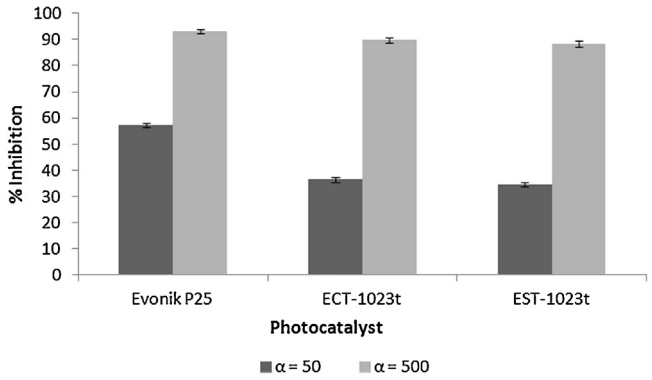


**Fig. 3.** % Inhibition due to the scavenger i-PrOH during the photocatalytic degradation of imazalil with $\alpha$ (mol/mol) the ratio scavenger over imazalil concentration.

influence the photooxidation of imazalil when considering these photocatalysts. Regarding Evonik P25, the degradation rate seems to increase with pH, and therefore adsorption (Fig. 2). This difference between the commercial photocatalyst and the lab-made ones has already been observed in a previous study [25]. In this work is confirmed (Fig. 3) that the lab-made photocatalysts produce more •OH radicals than Evonik P25, as was already proved in other studies [31], because the lab-made photocatalysts provide higher degradation rates than Evonik P25 at pH values where the adsorption capacity for imazalil is very weak. To confirm this, the radical scavenger isopropanol (i-PrOH) has been added to the system at pH $3.8 \pm 0.1$, where adsorption of imazalil is negligible.

i-PrOH is known to be a good hydroxyl radical scavenger and is used to discriminate between direct oxidation with positive holes and the degradation with hydroxyl radicals in solution [32–34]. Different concentrations of i-PrOH were dosed to evaluate the effect on the heterogeneous photocatalytic degradation of imazalil (Fig. 3) and adsorption measurements (not shown) demonstrated that the presence of 10–100 mM i-PrOH has negligible influence on the adsorption of imazalil; therefore, i-PrOH cannot compete for the adsorption sites with imazalil.

From Fig. 3 we can observe a marked decrease in imazalil degradation for all photocatalysts in presence of an excess i-PrOH at pH $3.8 \pm 0.1$. The inhibition of the degradation reaction that takes place when this radical scavenger is introduced into the reaction system is evidently more significant for the photocatalyst Evonik P25 than for ECT-1023t and EST-1023t. This confirms that at pH $3.8 \pm 0.1$ the lab-made photocatalysts produce more reactive radicals such as •OH, and that these radicals play an important role in the degradation of imazalil.

On the other hand, a higher TOC removal was achieved at pH 5.0 for Evonik P25 and EST-1023t, in comparison to ECT-1023t (Fig. 2). This depends on many factors, which include the degradation mechanism of the photoproducts generated along the reaction. Based on the higher mineralization achieved with Evonik P25 and EST-1023t, the rest of the studies were carried out at pH 5.0 with these two photocatalysts.

### 3.4. Effect of photocatalyst load

Degradation rates can vary significantly as a function of catalyst load [35]. Fig. 4 shows that the apparent degradation rate constants ($k_{IMS}$) and the mineralization increase with the photocatalyst load up to 1.0 g/L for Evonik P25 and up to 2.5 g/L for EST-1023t. Above these photocatalyst loads, $k_{IMS}$ falls, probably due to scattering effects, where the agglomeration of particles prevents the absorption of light by the photocatalyst.

We can also observe that the lab-made catalyst, EST-1023t, is more efficient than commercial Evonik P25 at higher catalyst loads, but less effective at catalyst loads below 0.25 g/L. The lower efficiency presented by EST-1023t at smaller loads can be related to the large aggregate size of this material when suspended in water,

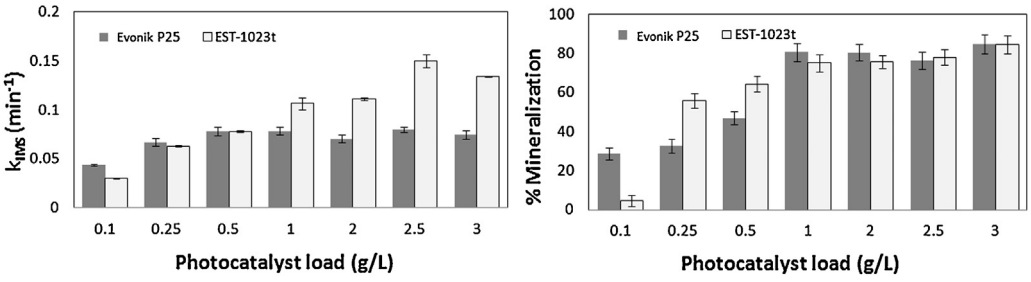


**Fig. 4.** Effect of photocatalyst load on apparent initial rate constant (left) and mineralization (%) after 2 h (right) for 50 mg/L imazalil at pH 5.0.

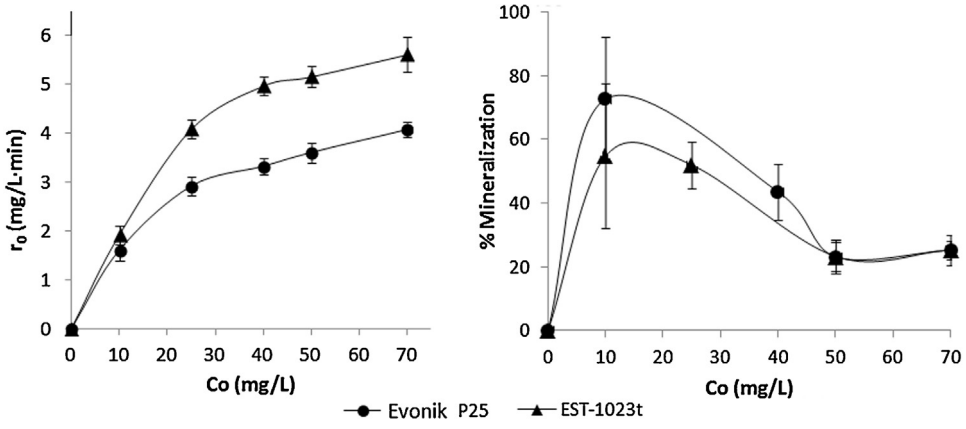


**Fig. 5.** Initial degradation rate, $r_0$ (left) and % mineralization in 45 min of irradiation (right) vs. $C_0$ for Evonik P25 and EST-1023t.

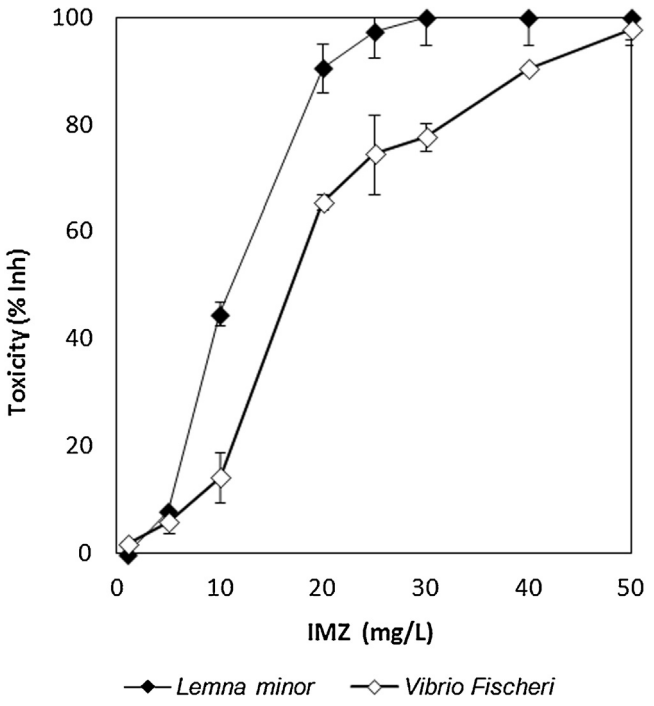


**Fig. 6.** Toxicity of imazalil to *Vibrio fischeri* and to *Lemna minor*.

as can be observed in Table 2, which could lead to a lower photonic yield when low loads are used. On the contrary, at higher photocatalyst loads, EST-1023t is more efficient than Evonik P25, probably due to a smaller light scattering effect at high catalyst loads [14].

### 3.5. Effect of initial imazalil concentration

The effect of initial imazalil concentration on the apparent degradation rate constant at pH 5.0 was studied up to 70 mg/L of imazalil with a comparable catalyst load (1 g/L) for Evonik P25 and EST-1023t (Fig. 5). The degradation follows a pseudo-first-order kinetic. A gradual deceleration in the increase of the initial degradation rate was observed by increasing the initial imazalil concentration, regardless the photocatalyst used. This is due to an increase in the number of molecules (imazalil and degradation by-products) adsorbed on the photocatalyst. This can produce the partial blockage of active sites and prevent the efficient generation of radical species at the studied conditions. On the other hand, at higher imazalil initial concentrations and for a same photocatalyst load, the •OH radicals/imazalil ratio is lower.

Furthermore, it is noticeable that the initial degradation rate is always higher for the photocatalyst EST-1023t than for commercial Evonik P25. Regarding mineralization, we can observe in Fig. 4 that the photocatalyst P25 exhibits higher mineralization at lower initial imazalil concentrations. This may be due to the surface area

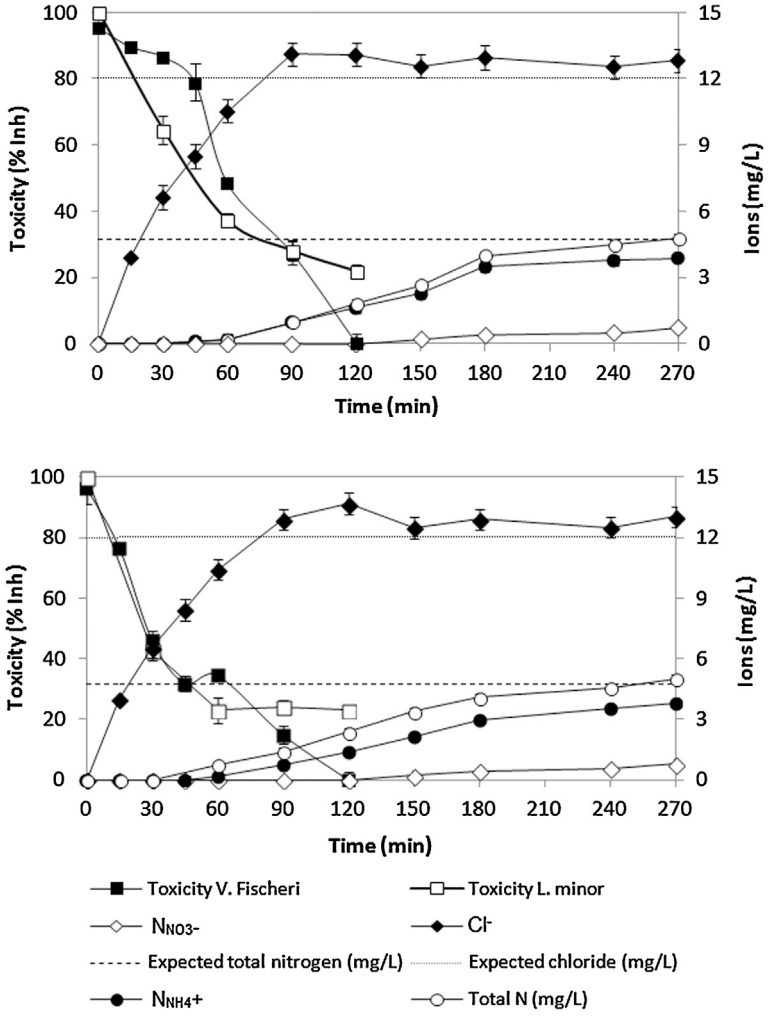


**Fig. 7.** Evolution of toxicity (left *y*-axis) and formation of ions (right *y*-axis) during imazalil photocatalytic degradation with commercial Evonik P25 (above) and EST-1023t (below) at a load of 1.0 g/L and pH 5.0.

of each photocatalyst that is available for the adsorption of intermediates, such as carboxylic acids, which are degraded by direct holes mechanism [36]. At the fixed photocatalyst load, Evonik P25 presents around 4 times more specific surface area than EST-1023t.

It should be also noticed that at higher imazalil initial concentrations both photocatalysts exhibit similar efficiencies due to the surface saturation.

### 3.6. Toxicity bioassay

Toxicity measurements are important in degradation reactions because in some cases the generated photoproducts can be more toxic than the parent compound [37]. In this context, Fig. 6 shows the toxicity to *V. fischeri* and to *L. minor* of different concentrations of imazalil and in Fig. 7 we can observe the changes produced in toxicity during the degradation process for 50 mg/L imazalil, at pH 5.0 and 1.0 g/L photocatalyst load.

Toxicity disappears for both photocatalysts after 120 min of irradiation. The toxicity reduction is faster with EST-1023t, in agreement with the results obtained above for imazalil degradation. However, from Figs. 6 and 7 we can see that not all the toxicity is related to imazalil. For instance, after 60 min of irradiation, the remaining imazalil for both photocatalysts is below 1 mg/L. At this concentration, imazalil is not toxic for *V. fischeri* or *L. minor*; however, the analyzed sample is still toxic. This toxicity is produced by the photoproducts generated during the reaction. For this reason, to study the possible intermediates produced in the degradation of imazalil is relevant.

On the other hand, *L. minor* seems to be a more sensitive species towards the photoproducts produced during the final stages of imazalil degradation, as we can observe from Fig. 6 that the toxicity reduction is not complete for this species.

### 3.7. Identification of degradation products

In order to identify the principal photoproducts resulting from the degradation of imazalil, three complementary techniques were employed: LC–MS, ion chromatography and FTIR.

The overall oxidation reaction for imazalil should produce two moles of chloride and two moles of nitrogen-containing ions per mole of imazalil. We have followed the formation of these ions as possible final products of the degradation reaction. For this purpose, we continued the degradation reaction until almost complete mineralization of the solution (TOC < 3 mg/L). The results are shown in Fig. 7.

From Fig. 7 we can confirm a radical-nucleophilic aromatic substitution, due to the liberation of chloride ions along the degradation of imazalil. The expected chloride for the total mineralization of 50 mg/L imazalil is obtained after 120 min of irradiation.

On the other hand, heterocyclic nitrogen groups in imidazoles are usually converted into ammonium or nitrate ions via the formation of amines or hidroxylamines [38]. We can also observe from Fig. 7 that the liberation of the nitrogen atoms as nitrate is much slower than that observed for chlorides and seems to mainly occur after dechlorination. Nitrate ions appear in dissolution after all the expected chloride, and ammonium is released faster than nitrate. This has been also observed in other studies [34,39].

In addition, the toxicity drops by 70–80% when the complete dechlorination of imazalil is achieved (Fig. 7). Less than a half of the total nitrogen ions were observed at this reaction time. This suggests that the remaining toxicity at higher reaction times is not a cause of chlorinated compounds, but due to the presence of the possible remaining hydroxybenzenes or imidazole residual compounds.

On the other hand, the main degradation products formed were identified by LC–MS. The compounds found are listed in Table 3.

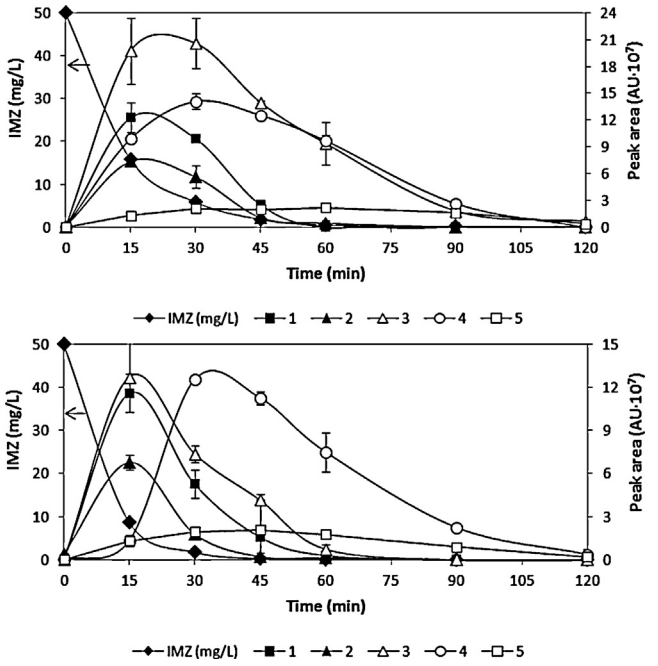


**Fig. 8.** Evolution of the identified photoproducts vs remaining imazalil at different reaction times for the photocatalysts Evonik P25 (above) and EST-1023t (below) at a load of 1.0 g/L and pH 5.0.

Some other studies have reported photoproducts for the elimination of imazalil [34,40–42], which include compound II and a variation of compounds I and III, in agreement with our studies. However, due to the different degradation conditions employed in the present study, compared to those found in literature mentioned above, other photoproducts were identified in the present study.

Fig. 8 shows the evolution of the degradation products during the photocatalytic degradation of imazalil. The identified photoproducts disappear after 120 min irradiation. The remaining TOC at this time (4.72 mg/L for Evonik P25 and 6.67 mg/L for EST-1023t) corresponds to other products that were not identified in this study, probably amines, hydroxybenzenes and carboxylic acids. Product IV is produced after the maximum amount of products I, II and III, and is degraded slower by using EST-1023t as catalyst. This fact confirms that this photocatalyst is less efficient than P25 for the degradation of adsorbed substrates.

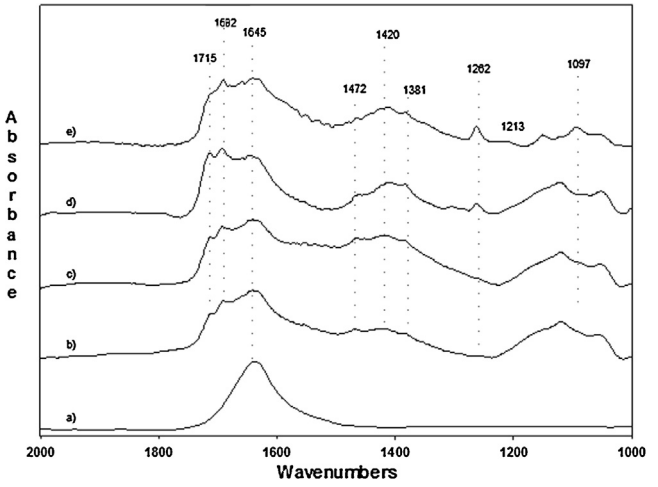


**Fig. 9.** FTIR spectra from interaction of imazalil and its photoproducts with Evonik P25 after adsorption equilibrium (b); and 60 (c), 120 (d) and 240 (e) min irradiation. (a) Represents the spectra of the photocatalyst alone.

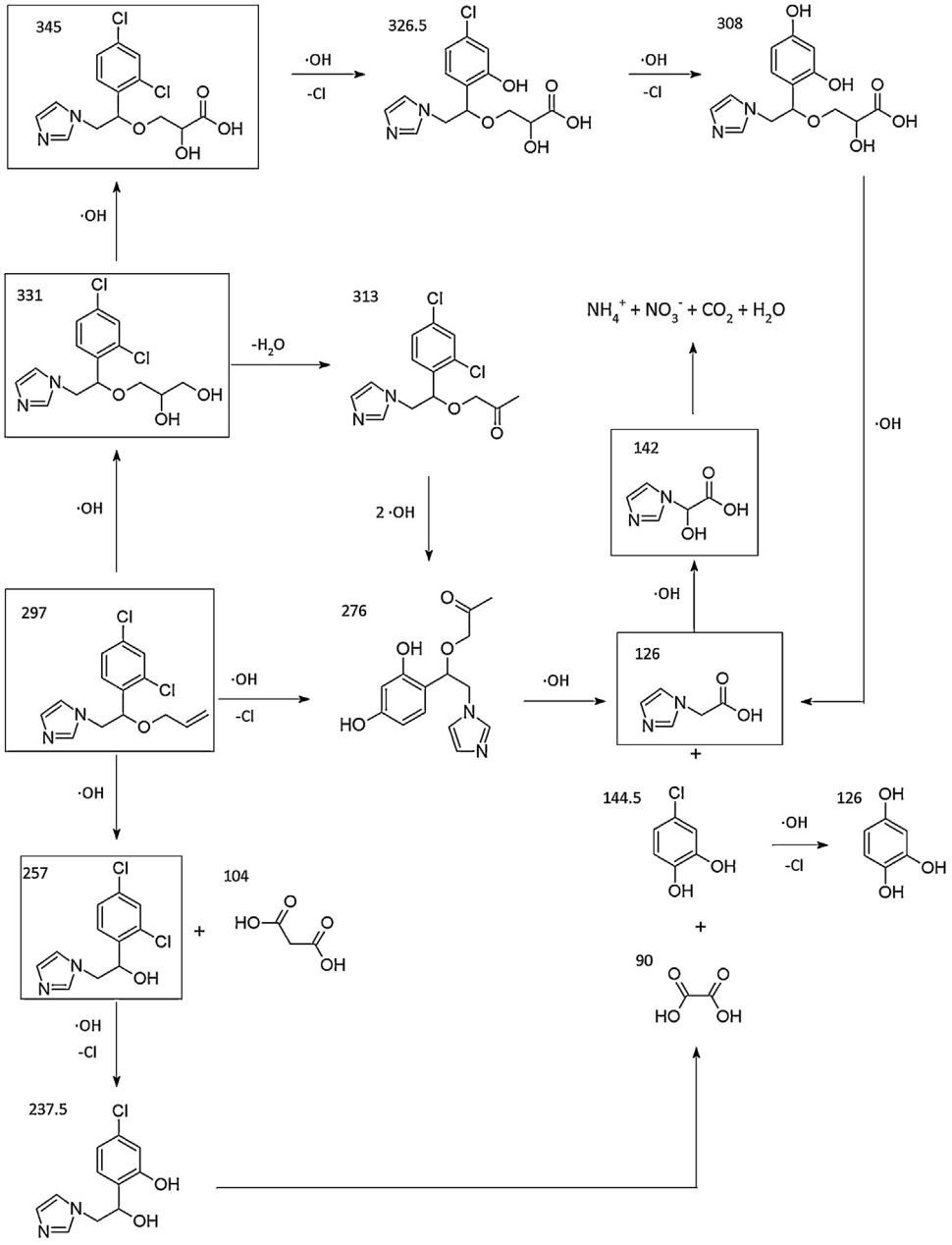


**Scheme 2.** Mechanism pathway proposed for the photocatalytic degradation of imazalil.

FTIR studies were rehearsed at different reaction times, for the photocatalytic degradation of imazalil, with the aim to obtain complementary information on the imazalil degradation pathway. Fig. 9 shows a gradual increase in the intensity of the bands located at 1715, 1692, 1472, 1420, 1381, 1262, 1213 and 1097 $cm^{-1}$ when the reaction time increases. The bands at 1715 and 1692 $cm^{-1}$ are attributed to $\nu$(C=O) vibration, the broad band at 1645 $cm^{-1}$ is related to water and $\nu$(C=N) vibration, the band at 1472 $cm^{-1}$ is sign of $\nu(CH_2)$ and the one at 1262 $cm^{-1}$ represents the $\nu$(C–O) group. Therefore, the spectra are progressively indicating the presence of imidazole acetic acids on the catalyst surface [43–45], in agreement with products IV and V shown in Table 3.

Considering the above, we have proposed a mechanism pathway for the photocatalytic degradation of imazalil, which is summarized in Scheme 2. As shown, the three degradation pathways produce the same final photoproduct.

In the first pathway, product with $m/z$ 257 is obtained by hydroxyl or any other oxidizing species attack on the ether [45]. This alcohol has been previously reported [34,42] and is rapidly oxidized. The remaining alquilic chain is probably oxidized to a carboxylic acid by the anti-Markovnikov mechanism.

In agreement with Fig. 9, a radical-nucleophilic aromatic substitution takes place. A further attack of hydroxyl radicals results in products IV and V.

The later opening of the imidazole ring has been reported in other studies [34]. Although we have not been able to identify the corresponding photoproducts with our LC–MS conditions, we have confirmed the rupture of the imidazole by ion chromatography, as shown in Fig. 8.

The other two proposed pathways consist on the hydroxylation of imazalil before the attack on the ether. These pathways lead to product I.

**Table 3**
Photoproducts identified from the degradation of imazalil.

| Number | Structure | *m*/*z* | Fragments (collision potential) |
|---|---|---|---|
| I | 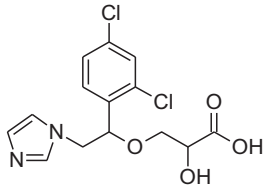 | 345 | 81.9 (15.5 V), 171.9 (22.5 V), 239.9 (10.5 V) |
| II | 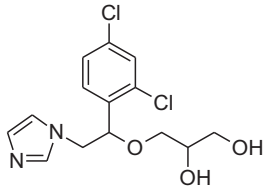 | 331 | 68.9 (15.5 V), 124.9 (31 V), 202.9 (15.5 V) |
| III | 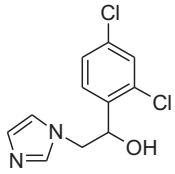 | 257 | 69.2 (12 V), 124.2 (30.5 V), 160.7 (20 V) |
| IV | 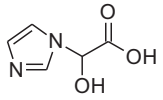 | 142 | 110.9 (10.5 V), 81.3 (28 V), 83.0 (19 V) |
| V | 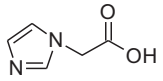 | 126 | 58.6 (18.5 V), 81.1 (19.5 V), 109.1 (12 V) |

## 4. Conclusions

The efficiency of heterogeneous photocatalysis for decontamination of waters containing imazalil was demonstrated in this study. The efficiency in imazalil degradation was correlated to different properties of the different studied photocatalysts, such as particle size, surface area, scattering effect and fungicide adsorption. The capacity to degrade imazalil increased with higher $TiO_2$ particle size. For this reason, the imazalil degradation is faster with the new home-made EST-1023t photocatalyst than with commercial Evonik P25.

The photocatalytic removal and mineralization of imazalil was influenced by the irradiation time, pH, initial imazalil concentration and photocatalyst load, and studies were performed to optimize these parameters. At different pH values, it was proved that adsorption is not an important step in the removal of imazalil and that the higher mineralization was obtained with Evonik P25 and EST-1023t at pH 5.0, in comparison to ECT-1023t. The photocatalyst Evonik P25 exhibits higher mineralization at lower initial imazalil concentrations due to its higher surface area for the adsorption of intermediates, such as carboxylic acids. However, EST-1023t is in general more efficient that Evonik P25 for catalyst loads higher than 0.25 g/L, and at the same catalyst load of 1.0 g/L, the lab-made catalyst EST-1023t is more efficient in the degradation of imazalil than the commercial Evonik P25, regardless the initial fungicide concentration used (up to 70 mg/L).

A detailed study on the photocatalytic degradation of imazalil was presented, including the identification of by-products. The formation of imidazole acetic acids along the reaction was confirmed by LC–MS and FTIR studies. Complete mineralization was achieved and confirmed by TOC analysis as well as the release of the stoichiometric nitrogen and chloride ions.

## Acknowledgements

We are grateful for the funding of the Spanish Ministry of Economy and Competitiveness through NANOBAC Project (ref. IPT-2011-1113-310000). Furthermore, we wish to thank the Spanish Ministry of Science and Innovation for their financial support through the Project CTQ2011-26617-C03-01, to the Universidad de Las Palmas de Gran Canaria for the funding through the PhD Grant Program and to the Banana Producers Association of Gran Canaria (Spain). AMTS acknowledges support from PEst-C/EQB/LA0020/2011 financed by FEDER through COMPETE and by FCT – Fundacão para a Ciência e a Tecnologia.

## Appendix A. Supplementary data

Supplementary data associated with this article can be found, in the online version, at http://dx.doi.org/10.1016/j.apcatb.2013.03.024.

## References

[1] DOUE, Reg. 97/73/EC, L 353 (1997) 26–28.
[2] DOUE, Reg. 396/2005/EC, L70 (2005) 1–16.
[3] BOE, Real Decreto 849/1986, vol. 103 (1986) 15500–15537.
[4] BOC, Decreto 82/1999, vol. 73, no. 73 (1999) 8382–8436.
[5] Coplaca Pudrición de corona en el plátano canario (2004).
[6] J. Araña, C. Garriga, C. Fernandez Rodriguez, J.A. Herrera Melian, J.A. Ortega Mendez, J.M. Doña Rodriguez, J. Perez Peña, Chemosphere 71 (2008) 788–794.

[7] D.E. Santiago, E.P. Melián, C.F. Rodríguez, J.A. Ortega Méndez, S.O. Pérez-Báez, J.M. Doña-Rodríguez, Green and Sustainable Chemistry 1 (3) (2011) 39–46.
[8] J.A. Arroyave Rojas, L.F. Garcés Giraldo, A.F. Cruz Castellanos, Revista Lasallista de Investigación 3 (2) (2006) 19–24.
[9] J.A. Arroyave Rojas, L.F. Garcés Giraldo, A.F. Cruz Castellanos, Revista Lasallista de Investigación 4 (1) (2007) 1–7.
[10] S. Malato, J. Blanco, J. Cáceres, A.R. Fernández-Alba, A. Agüera, A. Rodrıĭguez, Catalysis Today 76 (2–4) (2002) 209–220.
[11] A.G. Agrios, P. Pichat, Journal of Photochemistry and Photobiology A: Chemistry 180 (2006) 130–135.
[12] H.-H. Ou, S.-L. Lo, Journal of Molecular Catalysis A: Chemical 275 (2007) 200–205.
[13] E. Pulido Melián, O. González Díaz, J.M. Doña Rodríguez, G. Colón, J.A. Navío, M. Macías, J. Pérez Peña, Applied Catalysis B: Environmental 127 (2012) 112–120.
[14] J. Araña, J.M. Doña-Rodríguez, D. Portillo-Carrizo, C. Fernández-Rodríguez, J. Pérez-Peña, O. González Díaz, J.A. Navío, M. Macías, Applied Catalysis B: Environmental 100 (2010) 346–354.
[15] O. Carp, C.L. Huisman, A. Reller, Progress in Solid State Chemistry 32 (2004) 33–177.
[16] M. Maicu, M.C. Hidalgo, G. Colón, J.A. Navío, Journal of Photochemistry and Photobiology A: Chemistry 217 (2–3) (2011) 275–283.
[17] Y. Ito, Y. Ikai, H. Oka, J. Hayakawa, T. Kagami, Journal of Chromatography A 810 (1998) 81–87.
[18] H.-C. Su, A.-Y. Lin, Journal of Food and Drug Analysis 11 (4) (2003) 296–301.
[19] M. Bavcon Kralj, P. Trebse, M. Franko, Trends in Analytical Chemistry 26 (11) (2007) 1020–1031.
[20] American Public Health Association (APHA), Standard Methods for the Examination of Water and Wastewater, 21st ed., American Public Health Association (APHA), Washington, DC, 20058–63.
[21] J. Rivera-Utrilla, I. Bautista-Toledo, M.A. Ferro-García, C. Moreno-Castilla, Journal of Chemical Technology & Biotechnology 76 (2001) 1209–1215.
[22] European Commision, Health & Consumer Protection Directorate, Imazalil 1688/VI/97 (2007) 1–15.
[23] FAO, Specifications and evaluations for plant protection products, Imazalil (2001) 1–27.
[24] Z. Ambrus, K. Mogyorósi, A. Szalai, T. Alapi, K. Demeter, A. Dombi, P. Sipos, Applied Catalysis A: General 340 (2008) 153–161.
[25] C. Fernández-Rodríguez, J.M. Doña-Rodríguez, O. González-Díaz, I. Seck, D. Zerbani, D. Portillo, J. Perez-Peña, Applied Catalysis B: Environmental 125 (2012) 383–389.
[26] G. Li, C.P. Richter, R.L. Milot, L. Cai, C.A. Schmuttenmaer, R.H. Crabtree, G.W. Brudvig, V.S. Batista, Dalton Transactions 45 (2009) 10078–10085.
[27] H.K. Singh, M. Saquib, M.M. Haque, M. Muneer, D.W. Bahnemann, Journal of Molecular Catalysis A: Chemistry 264 (2007) 66–72.
[28] European Food Safety Authority (EFSA), EFSA Journal 8 (3) (2010) 1–67.
[29] P. Mazellier, É. Leroy, B. Legube, Journal of Photochemistry and Photobiology A: Chemistry 153 (2002) 221–227.
[30] A. Bhatnagar, P.K. Sharma, N. Kumar, International Journal of Pharmtech Research 3 (1) (2011) 268–282.
[31] L.M. Pastrana-Martínez, J.L. Faria, J.M. Doña-Rodríguez, C. Fernández-Rodríguez, A.M.T. Silva, Applied Catalysis B: Environmental 113–114 (2012) 221–227.
[32] X. Van Doorslaer, P.M. Heynderickx, K. Demeestere, K. Debevere, H. Van Langenhove, J. Dewulf, Applied Catalysis B: Environmental 111–112 (2012) 150–156.
[33] Y. Chen, S. Yang, K. Wang, L. Lou, Journal of Photochemistry and Photobiology A: Chemistry 172 (2005) 47–54.
[34] R. Hazime, C. Ferronato, L. Fine, A. Salvador, F. Jaber, J.M. Chovelon, Applied Catalysis B: Environmental 126 (2012) 90–99.
[35] E.I. Seck, J.M. Doña-Rodríguez, C. Fernández-Rodríguez, O.M. González-Díaz, J. Araña, J. Pérez-Peña, Chemical Engineering Journal 203 (2012) 52–62.
[36] D.W. Bahnemann, S.N. Kholuiskaya, R. Dillert, A.I. Kulak, A.I. Kokorin, Applied Catalysis B: Environmental 36 (2002) 161–169.
[37] J.A. Zazo, J.A. Casas, A.F. Mohedano, M.A. Gilarranz, J.J. Rodríguez, Environmental Science & Technology 39 (2005) 9295–9302.
[38] K. Nohara, H. Hidaka, E. Pelizzetti, N. Serpone, Journal of Photochemistry and Photobiology A: Chemistry 102 (1997) 265–272.
[39] S. Malato, Innovative Processes and Practices for Wastewater Treatment and Reuse, Turkey, 2007.
[40] E.M. Thurman, I. Ferrer, J.A. Zweigenbaum, J.F. García-Reyes, M. Woodman, A.R. Fernández-Alba, Journal of Chromatography A 1082 (2005) 71–80.
[41] A.K. Genena, D.B. Luiz, W. Gebhardt, R.F.P.M. Moreira, H.J. José Horst, Fr Schröder, Ozone: Science & Engineering 33 (2001) 308–328.
[42] A.K. Genena, Tratamento de Efluente Agroindustrial Contend Compostos Persistentes por meio dos Processos de Coagulaçao-floculaçao, Fenton, Foto-Fenton, Foto-peroxidaçao e Ozonizaçao, Universidade Federal de Santa Catarina, Florianópolis, 2009.
[43] N.B. Colthup, L.H. Daly, S.E. Wiberley, Introduction to Infrared and Raman Spectroscopy, 3rd ed., Academic Press, New York, 1990, 547 pp.
[44] C. Pouchert, Aldrich Library of Infrared Spectra, 3rd ed., Aldrich Chemical Co, Milwaukee, 1981, 1850 pp.
[45] Meislich, Química Orgánica, 3rd ed., McGraw-Hill, Bogotá, 1992, 355 pp.